ACTIVE FLUTTER SUPPRESSION FOR NONLINEAR AEROELASTIC SYSTEM

Takanori DEGAKI
Department of Aeronautics and Astronautics, University of Tokyo,
Hongo, Bunkyo-ku, Tokyo 113-8656, Japan

Keywords: *Aeroservoelasticity, Transonic Flutter, CFD, Sliding Mode Control*

Abstract

This paper describes two-dimensional active flutter suppression to cope with the transonic dip using sliding mode control. The airfoil has plunge and pitch degrees of freedom with leading and trailing edge control surfaces. The aerodynamic forces acting on the airfoil, lift and pitching moment, are calculated by solving Euler's equations using computational fluid dynamics. At a specific altitude, flutter occurs between Mach number of 0.7 and 0.88, which corresponds to the transonic dip. Sliding mode control makes the airfoil to be stable all through the Mach number of flutter occurrence. Sliding mode controller gives wider flutter margin than linear quadratic regulator. These characteristics indicate that sliding mode control is useful for active flutter suppression in the transonic flight.

Nomenclature

a_h : nondimensional elastic axis location measured from midchord
a_∞ : speed of sound
b : semichord of the airfoil
C_l , C_m : lift and moment coefficients about the elastic axis, respectively
$C_{l\alpha}$, $C_{m\alpha}$: lift and moment coefficients about the elastic axis per angle of attack, respectively
$C_{l\beta}$, $C_{m\beta}$: lift and moment coefficients about the elastic axis per trailing edge deflection, respectively
$C_{l\delta}$, $C_{m\delta}$: lift and moment coefficients about the elastic axis per leading edge deflection, respectively
h : plunge displacement
I_α : moment of inertia of the airfoil about the elastic axis
k : control gain of switching function of the sliding mode controller
k_h , k_α : structural spring constant in plunge and pitch
L : lift per unit span
M : Mach number
M_y : pitching moment per unit span
m : mass of the airfoil per unit span
Q : weight matrix
r_α : radius of gyration of the airfoil about the elastic axis, $\sqrt{I_\alpha / (mb^2)}$
t : time
t_s : time, at which the states reach the final intersection of the sliding surfaces
U : freestream speed
$\overline{U}$: nondimensional speed, $U / b\omega_\alpha$
u : control inputs
x : states
x_α : nondimensional distance from the elastic axis to the center of mass
α : pitch angle
β : trailing edge flap angle
δ : leading edge flap angle
μ : mass ratio, $m / (\pi\rho b^2)$
τ : nondimensional time, tU / b
ω_h , ω_α : uncoupled natural frequencies associated with plunge and pitch degree of freedom, respectively, $\sqrt{k_h / m}$, $\sqrt{k_\alpha / I_\alpha}$
ξ : nondimensinal plunge, h / b

1 Introduction

An aircraft cruising at supersonic speed has the aeroelastically severest point in the transonic. Although the aircraft passes through the transonic region instantly, its structural stiffness is targeted for that region. This is because the critical speed of flutter suddenly drops in that region. We call this drop by transonic dip. If we can manage only the while of passing through the transonic dip using an active control, we can relax the restriction about the stiffness and reduce the weight of the aircraft.

When we consider the active flutter suppression at the transonic speed, two questions arise: how to design a controller in spite of uncertain equations about the aerodynamic forces and how to validate the performance of the controller. For the first question, adaptive control and robust control are suggested. For the second question, experiments and computational fluid dynamics (CFD) are studied. Baldelli et al. [1] experimentally studied transonic flutter margin augmentation using H_∞ controller where aerodynamic forces are derived from doublet point method. Matsushita et al. [2] pointed out that although the transonic flutter occurring in their wind tunnel model was limit cycle oscillation, it was suppressed using optimal regulator with Kalman estimator. Fujimori et al. [3] carried out the transonic aerodynamic model modification and H_∞ controller used flutter suppression. From the results that the dynamic pressure of flutter boundary in the experiment was lower than that in the calculation, they suggested the change of wind tunnel test condition and the ability of the actuator must be considered for the controller design. A digital adaptive controller was introduced for active flutter suppression undergoing time varying flight conditions [4]. It was indicated that the parameter estimator possibly failed to follow the aeroelastic system change depending on the flight paths. Another adaptive control application for the transonic flutter suppression was carried out, in which CFD-based aerodynamic loads were used [5]. The adaptive controller was a good candidate for suppression of the transonic flutter associated with strong shocks.

We suggest sliding mode control [6], [7] as a potential solution for the system that has unknown dynamics including nonlinearity. If the model uncertainties are satisfied matching condition, the behavior of the system under sliding mode control has strong robustness. Since the aeroelastic system, in which the airfoil has leading and trailing edge control surfaces, satisfies this matching condition, we can expect the sliding mode controller to effectively suppress the transonic flutter of aerodynamic uncertainties involved. Furthermore, regarding the difference of the aerodynamic characteristic in Mach numbers as model uncertainties, we apply the sliding mode controller designed for a Mach number to the flutter suppression of another Mach number. This indicates that the sliding mode controller is effective all through the transonic dip.

In this study, we calculate the flutter speed of the airfoil NACA 64A006 in Mach number of 0.6 to 0.9. Considering a flight path at a constant altitude, we determine the Mach numbers, at which flutter occurs. Although the airfoil oscillates divergently between these Mach numbers, the sliding mode controller effectively suppress the flutter. We next confirm that the sliding mode controller can increase the flutter speed for all Mach numbers investigated. Compared to the linear quadratic regulator (LQR) of the same controller performance, the sliding mode controller provides much more margin to the critical speed.

2 Model and Equations of Motion

The two-dimensional wing section used in this study is shown in Fig. 1. This airfoil is supported by two springs, i.e., bending spring and torsional spring. Those two springs are simplification of the bending and torsional stiffness of a real three-dimensional wing. The plunge displacement h is positive downward and the pitch angle α is positive head up. The control surfaces for flutter suppression are the leading and trailing edges. Both are positive downward.

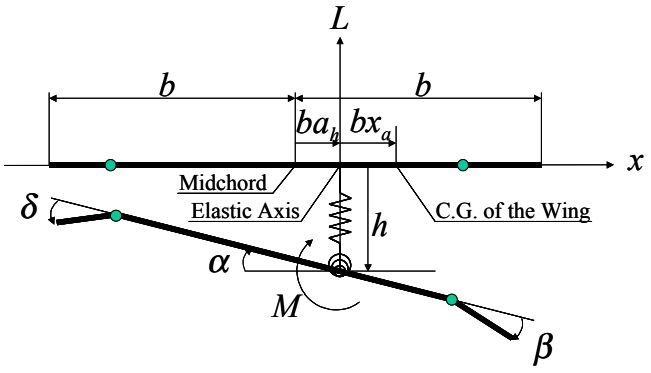

Fig.1 Two-dimensional wing section with leading and trailing edges. It is restrained from bending and torsional motion by two springs acting a distance *ba* aft of midchord. Lift and pitching moment about the elastic axis are shown.

The governing equations of the airfoil is

$$\begin{bmatrix} m & mx_\alpha \\ mx_\alpha & I_\alpha \end{bmatrix}\begin{Bmatrix} \ddot{h} \\ \ddot{\alpha} \end{Bmatrix}+\begin{bmatrix} k_h & 0 \\ 0 & k_\alpha \end{bmatrix}\begin{Bmatrix} h \\ \alpha \end{Bmatrix}=\begin{Bmatrix} -L \\ M_y \end{Bmatrix} \quad (1)$$

where the dot indicates the derivative with respect to time. In Eq.(1), we assume that a) the dynamics of leading and trailing edges are neglected, in other words the flaps perfectly track the reference inputs, b) reaction torque due to moving edges has no influence on the wing itself and c) the static moment and the moment of inertia of the wing section after the edge deflection are same as those before the edge deflection. We obtain a nondimensional form of Eq. (1) as follows:

$$\begin{bmatrix} 1 & x_\alpha \\ x_\alpha & r_\alpha^2 \end{bmatrix}\begin{Bmatrix} \xi'' \\ \alpha'' \end{Bmatrix}+\frac{1}{\overline{U}}\begin{bmatrix} (\omega_h/\omega_\alpha)^2 & 0 \\ 0 & r_\alpha^2 \end{bmatrix}\begin{Bmatrix} \xi \\ \alpha \end{Bmatrix}=-\frac{1}{\pi\mu}\begin{bmatrix} 1 & 0 \\ 0 & -2 \end{bmatrix}\begin{Bmatrix} C_l \\ C_m \end{Bmatrix} \quad (2)$$

where the prime indicates the derivative with respect to nondimensional time τ. The lift and moment coefficients are calculated by solving Euler's equation using CFD.

3 Sliding Mode Control

Sliding mode control is one of the variable structure controls. Unlike H_∞ control or μ-synthesis, sliding mode control is available even for nonlinear systems. Moreover sliding mode control accepts model uncertainties and parameter changes as far as they satisfy the matching condition.

Considering the flutter suppression, we encounter uncertainties about aerodynamics. If we use the simplified model like the quasi-steady aerodynamic theory and design a conventional controller, we may fail to suppress the flutter due to the difference between the simplified model and the real aerodynamic forces. One of the feasible control laws for such a purpose is sliding mode control.

In this study, we use the quasi-steady aerodynamic theory

$$\begin{aligned} C_l &= C_{l\alpha}(\alpha+\xi')+C_{l\beta}\beta+C_{l\delta}\delta \\ C_m &= C_{m\alpha}(\alpha+\xi')+C_{m\beta}\beta+C_{m\delta}\delta \end{aligned} \quad (3)$$

as nominal aerodynamic forces for controller design. Substituting Eq. (3) into Eq. (2), we obtain the aeroelastic system, including model errors about lift and itching moment, as follows:

$$[M]\{q''\}+[C]\{q'\}+([K_s]+[K_a])\{q\}=[G]\{u\}+\{\Delta_f\} \quad (4)$$

where

$$\begin{aligned} \{q\} &= [\xi \quad \alpha]^T \\ \{u\} &= [\beta \quad \delta]^T \\ [M] &= \begin{bmatrix} 1 & x_\alpha \\ x_\alpha & r_\alpha^2 \end{bmatrix} \\ [C] &= \frac{1}{\pi\mu}\begin{bmatrix} C_{l\alpha} & 0 \\ -2C_{m\alpha} & 0 \end{bmatrix} \\ [K_s] &= \frac{1}{\overline{U}^2}\begin{bmatrix} (\omega_h/\omega_\alpha)^2 & 0 \\ 0 & r_\alpha^2 \end{bmatrix} \\ [K_a] &= \frac{1}{\pi\mu}\begin{bmatrix} 0 & C_{l\alpha} \\ 0 & -2C_{m\alpha} \end{bmatrix} \\ [G] &= \frac{1}{\pi\mu}\begin{bmatrix} -C_{l\beta} & -C_{l\delta} \\ 2C_{m\beta} & 2C_{m\delta} \end{bmatrix} \end{aligned} \quad (5)$$

and $\{\Delta_f\}$ is model errors of aerodynamic forces. Equations (4) and (5) are transformed into the state space form as

$$\{x'\}=[A]\{x\}+[B]\{u\}+\{\Delta\} \quad (6)$$

where

$$\{x\}=\begin{bmatrix}\{q\}^T & \{q'\}^T\end{bmatrix}^T$$
$$[A]=\begin{bmatrix}[0] & [I]\\ -[M]^{-1}[K] & -[M]^{-1}[C]\end{bmatrix}$$
$$[B]=\begin{bmatrix}[0]\\ [M]^{-1}[G]\end{bmatrix} \quad . \qquad (7)$$
$$\{\Delta\}=\begin{bmatrix}\{0\}\\ [M]^{-1}\{\Delta_f\}\end{bmatrix}$$

We need no accurate information of how $\{\Delta_f\}$ is represented, except a rough estimate of upper bound of the norm of $\{\Delta_f\}$.

Now we assume that $\{\Delta\}$ satisfies the matching condition, i.e., there exists $\{\tilde{\Delta}\}$ that satisfies the equations of

$$\{\Delta\}=[B]\{\tilde{\Delta}\}. \qquad (8)$$

Considering Eqs.(7), we assure the existence of $\{\tilde{\Delta}\}$ as

$$\{\tilde{\Delta}\}=[G]^{-1}\{\Delta_f\} \qquad (9)$$

because the matrix $[G]$ is invertible. When the matching condition of Eq. (8) is satisfied, the sliding mode controller stabilizes the aeroelastic system under the model uncertainties $\{\Delta\}$.

The sliding mode control consists of two modes, i.e., the sliding mode and the reaching mode. The sliding mode, on one hand, assures the convergence to the origin if the state is kept in the final intersection of the sliding surfaces. The reaching mode, on the other hand, assures the convergence to the final intersection of the sliding surfaces even if there exists model uncertainties. We design those two modes in the following.

The purpose of sliding mode design is to find the sliding surfaces that assure the convergence to the origin. We use quadratic minimization method [6] to determine the surfaces. The objective function

$$J=\int_{t_s}^{\infty}\{x\}^T[Q]\{x\}d\tau \qquad (10)$$

is chosen to be minimized subject to keeping the state in the final intersection of the sliding surfaces. Following the similar procedure as linear quadratic regulator design and solving Riccati equation, we obtain the sliding surfaces that minimize Eq. (10) as

$$[S]\{x\}=0 \qquad (11)$$

where each row of $[S]$ includes normal vectors of sliding surfaces. In this study, there have two sliding surfaces since the wing section has two control inputs.

The purpose of reaching mode design is to find the control inputs that assure the convergence to the final intersection of the sliding surfaces. We use unit vector control method to determine the control inputs. Such control inputs are as follows:

$$\{u\}=-[S][A]\{x\}-k\{\sigma\}/\|\{\sigma\}\| \qquad (12)$$

where $\{\sigma\}$ is defined as

$$\{\sigma\}=[S]\{x\} \qquad (13)$$

and $[S]$ is normalized to satisfy the following relations:

$$[S][B]=[I] \qquad (14)$$

In reality, in order to avoid chattering motion, Eq. (12) is modified [8] using an infinitesimal real number ε as

$$\{u\}=-[S][A]\{x\}-k\{\sigma\}/\left(\|\{\sigma\}\|+\varepsilon\right). \qquad (15)$$

The control gain k is determined by considering the model uncertainties. As the result of applying Lyapunov stability theorem to the aeroelastic system, the control gain k must be

$$k>\|\{\tilde{\Delta}\}\|. \qquad (16)$$

If the control gain k can be extremely large and the control inputs have no limit or saturation, the controller, as far as the input matrix $[B]$ is reliable, works effectively for any inaccurate model. The control gain k, in reality, cannot be so large due to the controller saturation. That is to say that the robustness of the sliding mode controller against the model uncertainties depends on the magnitude of the control inputs available.

In the sliding mode controller design, the design factors are only $[Q]$ of Eq. (10)and k of Eqs. (15). For choosing $[Q]$, any positive definite matrix is acceptable. For choosing k,

however, it is insufficient only to be positive but it must satisfy the inequality of Eq. (16).

4 Simulation Results

4.1 Open-Loop Studies

The airfoil using in this study is NACA 64A006. The properties are a_h =-0.2, r_α =0.5, x_α =0.2 and ω_h / ω_α =0.3 [9]. The hinge axes of the leading and trailing edges are located at 20% and 75% of the chord, respectively. The computational grids around the airfoil are shown in Fig. 2. The grid is generated by solving Poisson equations iteratively [10], [11] from the initial grid generated using transfinite interpolation [10], [12]. The grid consists of 121 node points in circumference and 40 node points in radius. The far field boundary is located at 20 chords. Before simulating the transonic flutter and its control, we compare the results with another studies and validate the computational code with Refs. [9], [13], [14]. Now that the design point of the flutter suppression is M =0.85, μ =50 and $\overline{U}$ =3.4, the aerodynamic coefficients for the steady flow of M=0.85 are calculated using CFD as $C_{l\alpha}$ =14.4, $C_{l\beta}$ =8.90, $C_{l\delta}$ =-0.0148, $C_{m\alpha}$ =1.53, $C_{m\beta}$ =-0.355 and $C_{m\delta}$ =-0.279.

Figure 3 shows the pressure coefficient on the airfoil in the steady flow of M=0.88. Since this Mach number exceeds the critical Mach number, the shock is located at the 3/4 chord.

The flutter speed around the transonic region is determined using U-g method [15] as

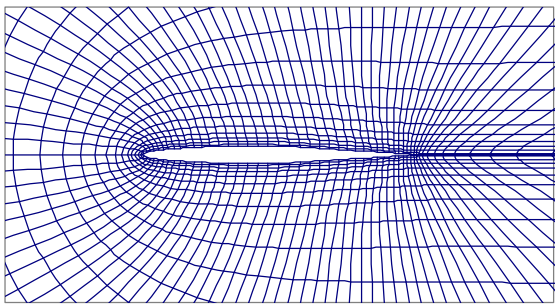

Fig.2 Body-fitted computational grid near the airfoil, NACA 64A006, before deformation.

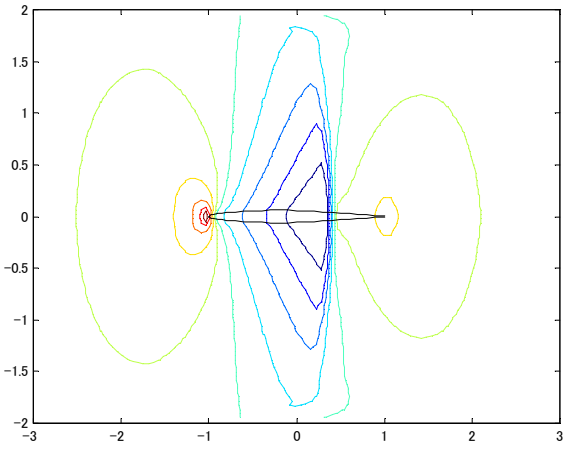

Fig.3 Pressure coefficient of the steady flow at M =0.88 with zero angle of attack.

shown in Fig. 4. In this region, the flutter speed varies remarkably and is accompanied by the dip. If we can specify the speed of sound correspond to the altitude, we draw the line of $\overline{U}$ - M relation in the figure of the flutter speed and determine the speed or Mach region at which flutter occurs. Provided that we assume $\overline{U}$ =4 M in Fig. 4, flutter occurs between 0.7 and 0.88 of Mach number. The corresponding speed is between $\overline{U}$ =2.8 and 3.52. Examples of the airfoil motions at some flutter Mach numbers are in Fig. 5. The initial condition is ξ'=-0.01/ $\overline{U}$, which is the same as Ref. [5]. At M =0.85, $\overline{U}$ =3.4 and a_∞ =340 m/s, it is equal to a vertical velocity change of 0.85 m/s. The oscillations of the airfoil are divergent after only a few cycles. We consider the suppression of those oscillations all through the flutter Mach numbers.

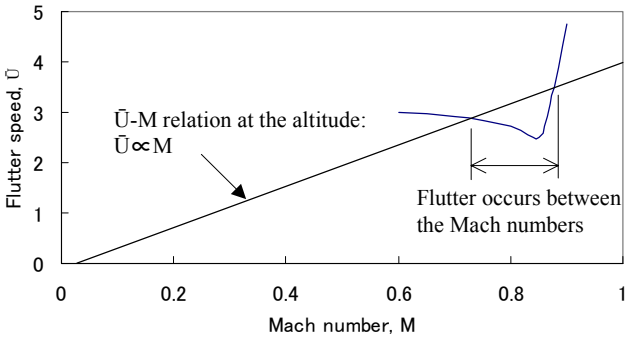

Fig.4 Flutter speed vs. Mach number for μ=50. Above the curve of the flutter speed, flutter occurs. The straight line represents flight at a particular altitude.

4.2 Closed-Loop Studies

Firstly we evaluate the magnitudes of those model uncertainties. The time histories of lift and pitching moment coefficients at the design point of M =0.85, corresponding plunge and pitch motions of which are in Fig. 5 c), are shown in Fig. 6. We assume the aerodynamic uncertainties have the same magnitude as the aerodynamic forces themselves. This assumption is overestimate of the model uncertainties and leads to conservative result about controller gain. Considering Eq. (9), we can find the norm of the lift and pitching moment as

$$\left\|\tilde{\Delta}\right\|=0.1, \qquad (17)$$

which means k must be 0.1 or more. We decide the lower bound of k for the purpose of avoiding the chattering motion:

$$k=0.1. \qquad (18)$$

Next we select a weighting matrix $[Q]$ as to minimize the time integral of the total energy, the kinetic energy and the potential energy, of the wing section all through the sliding mode. The total energy of the wing section is

$$\frac{1}{2}\{q\}^T[K_s]\{q\}+\frac{1}{2}\{q'\}^T[M]\{q'\}=\frac{1}{2}\{x\}^T\begin{bmatrix}[K_s] & [0]\\ [0] & [M]\end{bmatrix}\{x\} \qquad (19)$$

where the matrices $[M]$ and $[K_s]$ are in Eq. (5). That means

$$[Q]=\frac{1}{2}\begin{bmatrix}[K_s] & [0]\\ [0] & [M]\end{bmatrix}. \qquad (20)$$

Now we are ready to simulate and evaluate the closed-loop system. We apply the sliding mode control inputs of Eq. (15), which is designed by using Eqs. (18) and (20), to the aeroelastic airfoil in the freestream of M =0.70, 0.80, 0.85 and 0.88. The corresponding speed of those Mach number are $\bar{U}$ =2.8, 3.2, 3.4 and 3.52, respectively. Whereas the motion of the airfoil without the controller starting from the initial values of $\xi' = -0.01/\bar{U}$ is divergent as in Fig. 5, the motion of the airfoil with the sliding mode controller starting from the same initial values is suppressed effectively for all flight conditions throughout the transonic dip as in Fig.7.

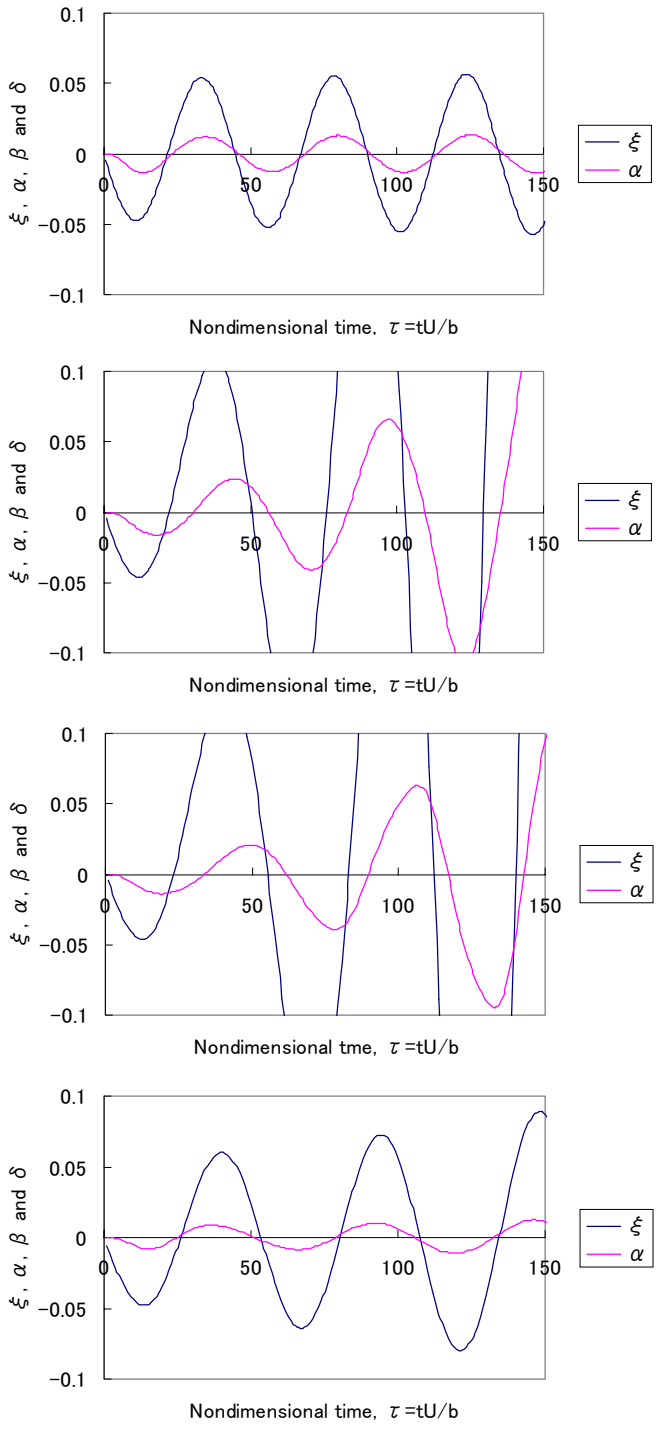

Fig.5 Time histories of plunge displacement and pitch angle without control at several Mach numbers; a) M=0.7, b) M=0.8, c) M=0.85 and d) M=0.88. The initial perturbation is plunge velocity of $-0.01b\omega_\alpha$, i.e., $d\xi/d\tau=-0.01/\bar{U}$.

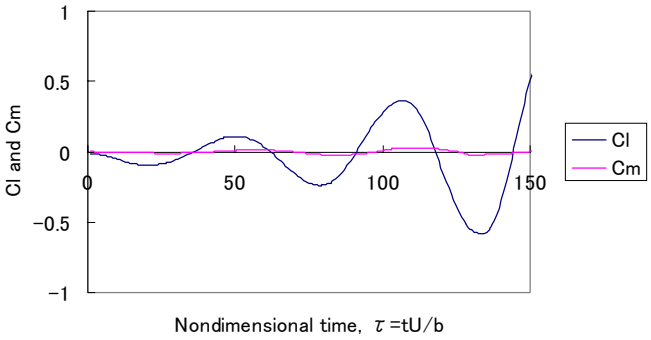

Fig. 6 Time histories of lift and pitching moment coefficients without control at Mach number of 0.85. The initial perturbation is the same as that in Fig. 5.

We also investigate the flutter margin of the airfoil with sliding mode controller in Fig. 8. The upper bound is more than $\overline{U}$ =20 or 30 (not shown in Fig. 8) and the lower bound is around $\overline{U}$ =0.5. Although the design point is M =0.85 and $\overline{U}$ =3.4, the sliding mode controller works effectively between those speeds at all Mach numbers.

We compare the performance of the sliding mode controller with the LQR. The objective function of the regulator is

$$J = \int_0^\infty \left(\{x\}^T [Q] \{x\} + 10^{-3} \{u\}^T \{u\} \right) d\tau . \quad (21)$$

The weight matrix to $\{x\}$ is the same as in Eq. (20), i.e., $\{x\}^T [Q] \{x\}$ represents the total energy of the airfoil. The weight to $\{u\}$ is chosen as to the time integral of the total energy $\int_0^\infty \left(\{x\}^T [Q] \{x\} \right) d\tau$ is equal to that of the sliding mode controller. At the design point, the LQR works effectively. The flutter margin, however, deteriorates, compared to the sliding mode controller, as shown in Fig. 9. While the lower bound is the same as that of the sliding mode controller, the upper bound deteriorates as to less than $\overline{U}$ =10. This indicates that the sliding mode controller is much more robust compared to the LQR.

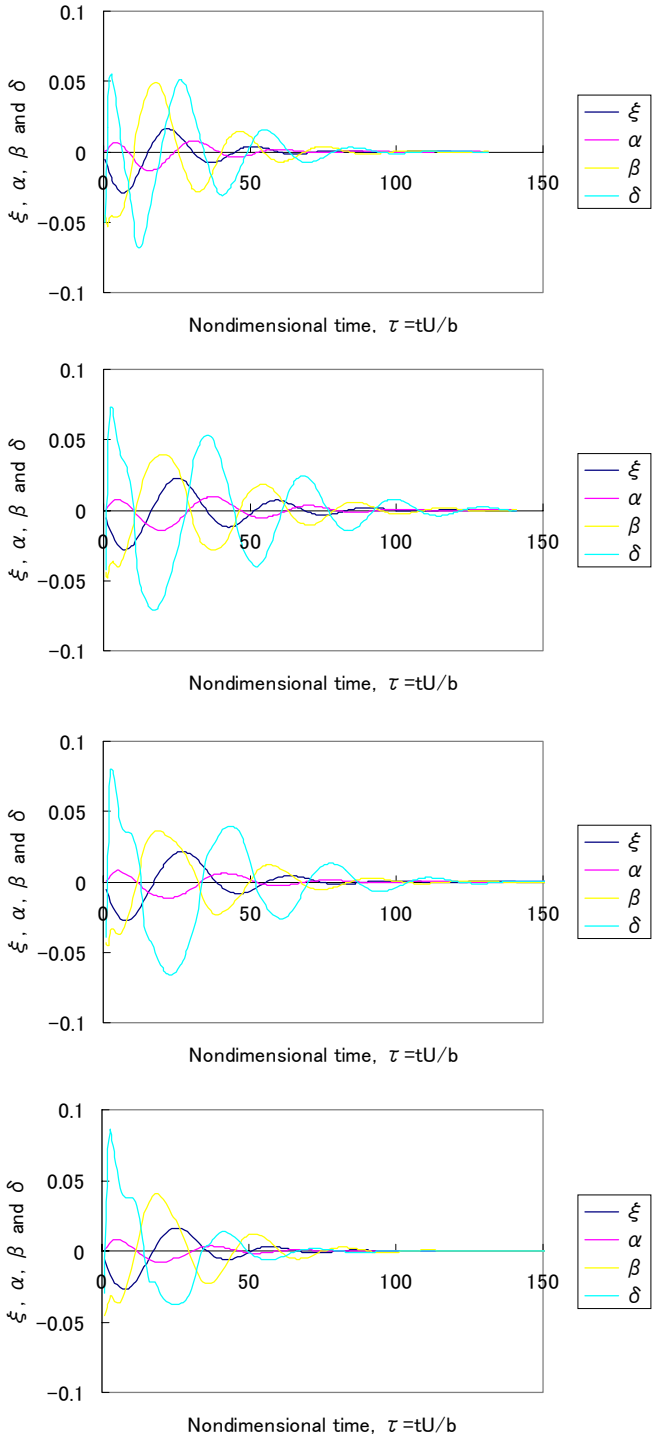

Fig. 7 Time histories of plunge, pitch, trailing and leading edges deformation using sliding mode control at several Mach numbers; a) M=0.7, b) M=0.8, c) M=0.85 and d) M=0.88. The initial perturbation is plunge velocity of $-0.01b\omega_\alpha$, i.e., $d\xi/d\tau=-0.01/\bar{U}$.

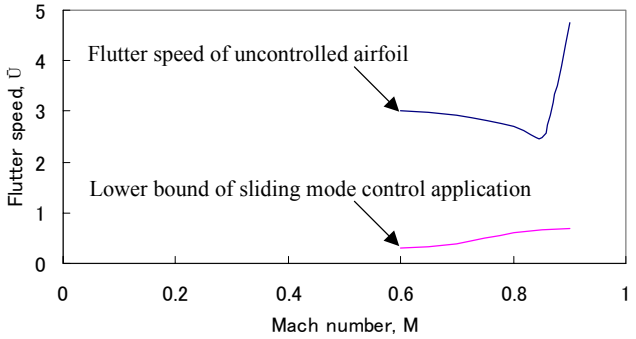

Fig. 8 Lower bound of the speed, above which the sliding mode controller is effective. Below the bound, the controller makes the airfoil diverge although the uncontrolled airfoil is stable. Upper bound is more than

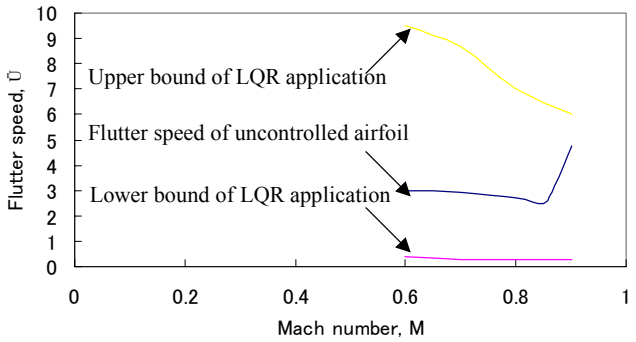

Fig. 9 Upper and lower bounds of the speed, between which the LQR is effective. Beyond the bounds, the controller makes the airfoil diverge. Also shown is flutter speed of uncontrolled airfoil.

5 Conclusions

We calculated using CFD the two-dimensional transonic flutter characteristics, in which the transonic dip appeared, and successfully suppressed the flutter by sliding mode control. The controller was effective for all the Mach numbers passing through the dip. Compared to LQR, the sliding mode controller possessed wider flutter margin.

Acknowledgement

The author wishes to thank Dr. Jiro Nakamichi and Dr. Hamid Kheiranfish in the National Aerospace Laboratory for their help with CFD computation.

References

[1] Baldelli D, Ohta H, Matsushita H, Hashidate M and Saitoh K. Flutter margin augmentation systhesis using normalized coprime factors approach. *Journal of Guidance, Control, and Dynamics,* Vol. 18, No. 4, pp. 802-811, 1995.

[2] Matsushita H, Saitoh K and Granasy P. Research on active control of aeroelastic systems at national aerospace laboratory in Japan. *International Journal of Intelligent Mechatronics,* Vol. 3, No. 1, pp. 34-51, 1998.

[3] Fujimori A, Matsushita A, Saitoh K and Ando Y. Model modification of a high-aspect-ratio aeroelastic wing and active flutter suppression. *Proceedings The 37th Aircraft Symposium,* Tokyo, 1C2, pp. 81-84, 1999 (in Japanese).

[4] Pak C, Friedmann P and Livne E. Digital adaptive flutter suppression and simulation using approximate transonic aerodynamics, *Journal of Vibration and Control,* Vol. 1, No. 4, pp. 363-388, 1995.

[5] Friedmann P, Guillot D and Presente E. Adaptive control of aeroelastic instabilities in transonic flow and its scaling, *Journal of Guidance, Control, and Dynamics,* Vol. 20, No. 6, pp. 1190-1199, 1997.

[6] Nonami K and Tian H. *Sliding mode control*. 1st edition, Corona Publishing, 1996 (in Japanese).

[7] Zinober A. *Deterministic control of uncertain systems*. Peter Peregrinus Ltd., 1990.

[8] Burton J and Zinober A. Continuous self-adaptive control using a smoothed variable structure. *International Journal of Systems Science,* Vol. 19, No. 8, pp. 1515-1528, 1988.

[9] Yang T and Chen C. Transonic flutter and response analyses of two 3-degree-of-freedom airfoil. *Journal of Aircraft,* Vol. 19, No. 10, pp. 875-884, 1982.

[10] Yasuhara M and Daiguji H. *Computational fluid dynamics,* 1st edition, University of Tokyo Publishing, 1992 (in Japanese).

[11] Steger J and Sorenson R. Automatic mesh-point clustering near a boundary in grid generation with elliptic partial differential equations. *Journal of Computational Physics,* Vol. 33, pp. 405-410, 1979.

[12] Eriksson L. Generation of boundary-conforming grids around wing-body configurations using transfinite interpolation, *AIAA Journal,* Vol. 20, No. 10, pp. 1313-1320, 1982.

[13] Yang T, Guruswamy P, Striz A and Olsen J. Flutter analysis of a NACA 64A006 airfoil is small disturbance transonic flow, *Journal of aircraft,* Vol. 17, No. 4, pp. 225-232, 1980.

[14] Tijdeman H. Investigation of the transonic flow around oscillating airfoils, NLR TR 77090 U, 1977.

[15] Washizu K. *Aeroelasticity,* 1st edition, Kyoritu Publishing, 1969 (in Japanese).